Protein stability modulated by a conformational effector: effects of trifluoroethanol on bovine serum albumin

Rita Carrotta,[a] Mauro Manno,*[a] Francesco Maria Giordano,[b] Alessandro Longo,[b] Giuseppe Portale,[c] Vincenzo Martorana[a] and Pier Luigi San Biagio[a]

Received 22nd October 2008, Accepted 5th February 2009
First published as an Advance Article on the web 5th March 2009
DOI: 10.1039/b818687a

The link between the thermodynamic properties of a solution and the conformational space explored by a protein is of fundamental importance to understand and control solubility, misfolding and aggregation processes. Here, we study the thermodynamic and conformational stability of a model protein, bovine serum albumin (BSA), by addition of trifluoroethanol (TFE), which is known to affect both the solvent properties and the protein structure. The solvent-mediated pair-wise interactions are investigated by static and dynamic light scattering, and by small angle X-ray scattering. The protein conformational details are studied by far- and near-UV circular dichroism (CD), and steady state fluorescence from tryptophan and from 1-anilino-8-naphthalene sulfonate (ANS). At low TFE concentrations, our results show that protein–protein interaction is dominated by steric repulsion accompanied by a consistent protein solvation. Minor local conformational changes also occur, but they do not affect the stability of BSA. At TFE concentrations above the threshold of 16% v/v, attractive interactions become prevalent, along with conformational changes related to a loosening of BSA tertiary structure. The onset of thermodynamic instability is triggered by the enhancement of hydrophobic attraction over repulsion, due to minor local changes of protein conformation and hydration. In the present context, TFE acts as a conformational effector, since it affects the intermolecular interaction and the activity of the proteins in solution through a direct mechanism.

I. Introduction

The thermodynamic and mechanical instability of protein solutions and the consequent protein aggregation are central issues in biotechnology, pharmaceutics and medical research.[1] They are important for drug design or to assess the shelf-life of pharmaceutical formulations,[2] as well as for the food industry and for the development of sustainable biocompatible materials.[3,4] Moreover, many systemic or neurodegenerative diseases are related to the misfolding and aggregation of proteins into amyloid fibrils.[5]

Nowadays, studies on protein crystallization and aggregation have disclosed compelling evidence that every protein can form different types of aggregates, depending upon the solution conditions and upon the protein conformational space explored.[5] For example, the crystal formation of native protein is prompted by the onset of mild protein attractive interactions,[6,7] joined to conditions stabilizing the native conformation.[8] Also, amyloid aggregation is often correlated to the stabilization of partially unfolded states.[5] In some cases, native proteins can form linear aggregates with amyloid morphology[9,10] sometimes after preliminary oligomer formation.[11] These results are of extreme interest since they highlight that the aggregation pathway may be independent from the unfolding pathway, and therefore the solution conditions should critically promote attractive intermolecular interactions.[12–14] Protein conformational details and solvent/co-solvent properties play a fundamental and interdependent role in determining solution stability and in understanding protein aggregation.[1,15–19]

The present study puts side by side the two intertwined aspects, which play a role in the understanding of protein stability and aggregation: solvent–co-solvent mediated protein–protein interactions and the co-solvent effect on protein conformation. Such a relation has still not been extensively studied, despite its pivotal relevance. Here, we study how 2,2,2-trifluoroethanol (TFE) affects the stability and the conformation of a model protein, bovine serum albumin (BSA). In order to address the effect of TFE on both interaction and conformation of BSA, we perform experiments at different TFE concentrations by different experimental techniques: far-UV and near-UV circular dichroism (CD); intrinsic tryptophan fluorescence and fluorescence of 1-anilino-8-naphthalene sulfonate (ANS); static and dynamic light scattering; and small angle X-ray scattering (SAXS).

TFE as a co-solvent favours both intra and intermolecular interactions. It is a less polar and weaker hydrogen bond

[a] *Institute of Biophysics at Palermo (IBF), Italian National Research Council, via U. La Malfa 153, I-90146, Palermo, Italy. E-mail: mauro.manno@pa.ibf.cnr.it; Fax: +39 (091) 680 9349; Tel: +39 (091) 680 9305*
[b] *Istituto per lo Studio dei Materiali Nanostrutturati, Palermo (ISMN), Italian National Research Council, via U. La Malfa 153, I-90146, Palermo, Italy*
[c] *Netherlands Organization for Scientific Research (NWO), DUBBLE CRG, ESRF, 6 rue Jules Horowitz, BP 220, F-38043, Grenoble Cedex 9, France*

donor than water, and its competition with water leads to a free energy decrease for the formation of intra or intermolecular hydrogen bonds. The effect of TFE on proteins strongly depends upon the TFE concentration and the specific protein. For example, TFE can strengthen α-helical secondary structures and/or favour formation of β-sheets. It is also used to stabilize the soluble structures of the peptides involved in the formation of amyloid fibrils. In general, TFE stabilizes the α-helical secondary structures in peptides[20,21] and protein.[22–24] As a consequence, it may modify the pathway of protein folding in opposite ways,[25] either enhancing the rate of protein folding,[26,27] or driving protein unfolding.[28,29] The latter may consist in the breakdown of the protein tertiary structure,[30] or in the generation of a molten globule structure,[31–33] or a partially folded conformation.[34,35]

The effect of TFE or other alcohols on the stability of protein solution is also remarkable. The overall effect of monohydric alcohols is to decrease protein conformation stability and to increase protein solution-phase stability.[8] At low alcohol concentration the solution-stabilizing effect dominates, while at high alcohol concentrations, the denaturing or destabilizing effect becomes overwhelming, leading in some cases to the formation of elongated fibrils.[8,9] In principle, the same mechanism that enhances folding,[25] should promote aggregation, at low TFE concentrations.[9,36] This effect has been related to protein selective hydration.[36,37] In such conditions, hydrophobic interactions are weakened due to the increase of the dielectric constant or to direct binding.[38]

The detailed mechanisms through which TFE affects protein conformation and stability are still controversial. They include direct mechanisms as preferential binding of TFE to the helical conformer of peptides[39] or preferential solvation of certain backbone groups by TFE.[36] Other proposed indirect mechanisms include the solvent-induced stabilization of the helical states by enhancing the polypeptide internal H-bonding or by disrupting the water structure and lessening the hydrophobic effect.[38,40] At very high concentration (30% and above), TFE may cluster to form clathrate hydrate-like aggregates,[41,42] or micro-heterogeneities,[43] which have been found to locally assist the folding of secondary structures.[44] The conformational transitions induced by TFE on a protein correlates with the extent of cluster formation.[45]

Our results show that up to a TFE concentration of 16% v/v, the solution stability is mainly controlled by steric repulsion with a significant contribution of molecular solvation. By further increasing TFE concentration, an attractive interaction becomes prevalent, eventually driving towards protein aggregation. At the molecular level, the present results show that only moderate changes in the BSA conformation occur, mainly related to a preferential hydration of protein surface by TFE,[36] which eventually determine a loosening of the hydrophobic pocket of BSA. Therefore, the increase in the hydrophobic surface of protein molecules gives a rationale for the onset of protein attraction and the loss of solution stability.

In other words, the onset of thermodynamic instability and intermolecular attraction is due to the balance of the interactions involved, and in particular to the strengthening of the hydrophobic interaction, which overcomes electrostatic repulsion.[8,38]

II. Experimental methods

A Sample preparation

All the chemicals were of analytical grade. BSA and TFE were purchased from SIGMA. BSA in 50 mM buffer phosphate (pH 6.2) was further purified using 100-kDa Centricon filters to get ride of covalently linked oligomers. Protein concentration was measured by using an extinction coefficient at 280 nm of 44 289 M^{-1} cm^{-1}. Samples at different TFE concentrations were prepared from a stock solution of 50% v/v TFE in 50 mM phosphate buffer (pH 6.2). Solutions were made by weight, assuming that the density of TFE is 1.373 g ml^{-1} and that of 50% v/v TFE solution is 1.217 g ml^{-1}.[43] A pH control of the solution 50% v/v TFE in 50 mM phosphate buffer pH 6.2 assured no change of pH due to the addition of TFE. All the solutions were filtered through a 0.2 μm Millex LG filter. TFE compatibility with the filters was preliminarily studied.

B Light scattering

The solutions were directly filtered into a quartz cuvette and placed in a thermostatically controlled cell compartment of a Brookhaven Instrument BI200-SM goniometer (set at 90°), equipped with a 100-mW Ar laser tuned at $\lambda_0 = 488$ nm. The temperature was set to 25 °C and controlled by a thermostated circulating bath with a tolerance of 0.05 °C. The scattered light intensity and its autocorrelation function were simultaneously measured by a Brookhaven Instrument BI9000 correlator. Absolute values for scattered intensity (Rayleigh ratio) were obtained by normalization with respect to toluene, whose Rayleigh ratio at 488 nm was taken as 39.6 10^{-6} cm^{-1}. The apparent diffusion coefficient D_{app}, was obtained from the intensity autocorrelation function by fitting to the expression $g_2(t) = 1 + \beta|\exp(-D_{app}q^2t)|^2$, where β is an instrumental factor, and q is the scattering vector $q = 4\pi\tilde{n}\lambda_0^{-1}\sin(\theta/2)$, which depends upon the scattering angle θ, the incident wavelength λ_0, and the refractive index of the medium $\tilde{n}$ (taken 1.33, for all the studied water/TFE solutions).

C Small angle X-ray scattering (SAXS)

X-Ray measurements were performed with the synchrotron beamline BM26B, DUBBLE, at the European Synchrotron Radiation Facilities (ESRF, Grenoble, France). Experiments were carried out using a monochromatic 12-keV X-ray beam. Scattering images were recorded by placing a two-dimensional position sensitive detector at a distance of 1.5 m from the sample. In order to obtain the isotropic SAXS intensity profiles, the dimensional images were radially averaged around the centre of the primary beam using FIT2D software. Silver behenate was used as standard to determine the centre of the beam and to calibrate the scattering vector scale. Each spectrum was at first normalized for the intensity of the incident beam and then, the scattering from the empty cell was subtracted after correction for transmission difference between the sample and the empty cell.

D Circular dichroism

Circular dichroism (CD) spectra were recorded by using a JASCO J-600 system. Far-UV CD spectra were measured in the range 200–250 nm by using a 0.2-cm optical path quartz cuvette and a protein concentration of 2.8 μM. Near-UV CD spectra were measured in the range 250–350 nm by using a 1-cm optical path quartz cuvette and a protein concentration 11.3 μM.

E Fluorescence

Intrinsic and 1-anilino-8-naphthalene sulfonate (ANS) fluorescence were measured on a JASCO FP-6500 spectrofluorimeter. Intrinsic fluorescence was measured on solutions of BSA concentration 2 μM. The tryptophan emission spectrum was measured at λ_{ex} = 290 nm, with a scan rate of 100 nm min^{-1}, excitation and emission slit width of 1 nm and 3 nm, respectively. The quantum yield was calculated by normalization of the integrated emission spectrum with the absorption corresponding to the excitation wavelength. The same experimental conditions were used for all the samples. The concentration of ANS was chosen as 100 μM with a ratio ANS-BSA of 50 : 1. The ANS emission spectrum was measured at λ_{ex} = 380 nm, scan rate 100 nm min^{-1}, excitation and emission slit width 5 nm.

III. Results and discussion

A Modulation of both protein conformation and interaction by TFE

In the present work, we study how TFE affects both the stability of BSA solution and the conformation of BSA molecules. The changes in the BSA conformation by addition of TFE are studied by far-UV and near-UV circular dichroism (CD), intrinsic tryptophan fluorescence and fluorescence of 1-anilino-8-naphthalene sulfonate (ANS), a probe with high affinity for hydrophobic protein environment. The protein interactions are studied by static and dynamic light scattering and by small angle X-ray scattering (SAXS).

B Static light scattering experiments

Static light scattering experiments were performed at different TFE concentrations from (0 to 23% v/v) and at different protein concentrations to measure the Rayleigh ratio at 90°, R_{90} (Fig. 1a). In dilute solutions, the dependence of R_{90} on protein mass concentration c yields the weight averaged molecular mass of BSA, M_w, and the osmotic second virial coefficient, B_2, according to the expression:[46]

$$\frac{KcM_w}{R_{90}} = 1 + 2B_2\rho \qquad (3.1)$$

where $\rho = N_A M_0^{-1} c$, the protein number concentration; N_A is Avogadro's number; M_0 is the protein molecular mass; and K is an instrumental constant $K = (2\pi\tilde{n}[d\tilde{n}/dc]\lambda_0^{-2})^2 N_A^{-1}$. Here, we take $[d\tilde{n}/dc] = 0.187$ mg^{-1} ml,[47] which holds for BSA in phosphate buffer solutions. Upon addition of TFE we do not expect appreciable changes within an error of 10%. Moreover, we are here assuming that the Rayleigh ratio does not depend upon the scattering angle θ. Indeed, the protein form factor can be taken as equal to 1, considering that the protein size is much less than the reciprocal of the scattering vector. Also, the structure factor can be reasonably taken as equal to 1 at such dilutions.[46] In Fig. 1a, the experimental data and the fitting functions are shown according to the expression (3.1). The average M_w in the measured range of TFE concentrations is $\langle M_w \rangle$ = 74 ± 7 kDa, which agrees with the nominal molar mass of BSA (66 430 kDa)[48] (inset of Fig. 1a).

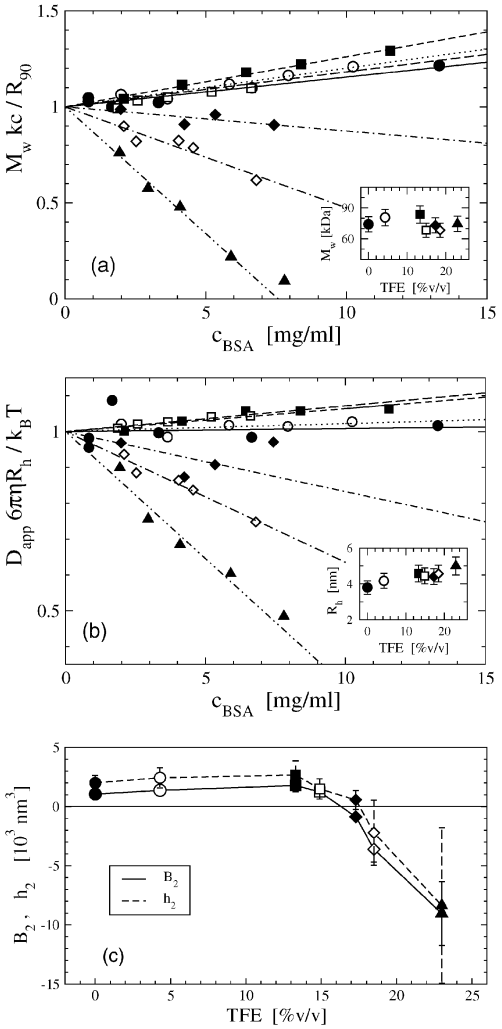

Fig. 1 Light scattering experiments at different BSA and TFE concentrations (the latter are identified by matching symbols): 0% (black circles), 4.3% (white circles), 13.3% (black squares), 14.9% (white squares), 17.3% (black diamonds), 18.5% (white diamonds), 23.0% (black triangles). (a) Rayleigh ratio measured by static light scattering, normalized as reported in the *y*-axis and in the text. Inset: Molecular mass *versus* TFE concentration. (b) Diffusion coefficient measured by dynamic light scattering, normalized as reported in the *y*-axis and in the text. Inset: Hydrodynamic radius *versus* TFE concentration. (c) Second virial coefficient and hydrodynamic coefficient *versus* TFE concentration.

The osmotic second virial coefficient B_2 is related to the two-body mean-field potential $U(r)$,[49] accounting for the interaction between two protein at a center-to-center distance r:

$$B_2 = 2\pi \int_0^\infty (1 - e^{-\beta U(r)}) r^2 \, dr \qquad (3.2)$$

where $\beta = (k_B T)^{-1}$.

The sign of B_2 is related to protein stability and solubility, depending upon the prevalence of repulsive or attractive interaction.[6,7,16,50,51]

C Dynamic light scattering experiments

Simultaneously with static light scattering, dynamic light scattering experiments were performed to measure the intensity autocorrelation function and to extract the apparent diffusion coefficient D_{app} (Fig. 1b). The dependence of D_{app} on protein concentration c yields the z-averaged hydrodynamic radius of BSA, R_h, and the hydrodynamic coefficient, h_2, according to the expression:[46,52]

$$\frac{D_{app}}{D_0} = 1 + (2B_2 - h_2)\rho \qquad (3.3)$$

where D_0 is the self diffusion coefficient at infinite dilution, which depends upon the medium viscosity η of the TFE–buffer solvent,[53] the temperature T, the Boltzmann constant k_B, and the hydrodynamic radius R_h, through the Stokes–Einstein relation: $D_0 = k_B T(6\pi\eta R_h)^{-1}$. In Fig. 1b, the experimental data and the fitting functions are shown according to the expression (3.3). The hydrodynamic radius R_h without TFE is $R_h^{0\%} = 3.8 \pm 0.4$ nm, which agrees with previous results obtained under similar conditions ($R_h = 3.4$ nm).[54] At higher TFE concentrations, a slight increase of R_h is observable (inset of Fig. 1b). This apparent swelling is likely due to the changes of the protein hydration and of the hydrodynamic properties. It should not be associated with protein unfolding, which would require more dramatic changes in these values.[55]

D Triggering of intermolecular attraction and the onset of thermodynamic instability

The first evident result of the present work is the transition of BSA solution from a thermodynamically stable phase to a metastable phase upon addition of TFE, highlighted by the change in the sign of the second virial coefficient. In the present experimental conditions, this phase transition occurs at a threshold TFE concentration of about 16% v/v.

The osmotic second virial coefficient B_2 and the hydrodynamic coefficient h_2 *versus* TFE concentration are displayed in Fig. 1c. The results show that without TFE the solution is thermodynamically stable ($B_2 > 0$). By increasing the TFE concentration up to 13% v/v the BSA solution becomes more stable, since the second virial coefficient exhibits a moderate increase. The hydrodynamic coefficient is also not null, fostering the existence of significant hydrodynamic interactions. A further increase in TFE leads to a drop off of B_2, going to negative values, at $c_{TFE} > 16\%$ v/v. Also h_2 turns to negative values for TFE concentrations higher than 18% v/v. However, this result could be affected by the lack of accuracy, which is implicit in the subtraction of the static term $2B_2$, when the experiments are performed in the metastable phase. The change of sign of B_2 marks a changeover in the interactions, from repulsive to attractive. At high TFE concentration, protein association eventually occurs, and the solution becomes turbid after several minutes. At TFE concentrations higher than 25% v/v and BSA concentrations higher than a few mg ml^{-1}, the rate of aggregation was too fast, and we were not allowed to measure thermodynamic quantities during such a short metastable phase.

E The nature of repulsive interactions

The two thermodynamic parameters measured by light scattering data, B_2 and h_2, displayed in Fig. 1c, can shed light on the origin of repulsive forces. The osmotic second virial coefficient is determined by the interaction potential among solute molecules (expression (3.2)).[49]

A main contribution to the interaction between two macromolecules is due to the bare steric repulsion. In analogy with the studies on colloidal solutions,[7,8,56] one may assume as a first approximation a pairwise isotropic repulsive potential $U_{hs}(r)$ between two proteins with a center-to-center distance r and an "equivalent" hard-sphere diameter σ:

$$U_{hs}(r) = \begin{cases} \infty, & r < \sigma \\ 0, & r >= \sigma \end{cases} \qquad (3.4)$$

In the case of an ideal system with a repulsive hard sphere potential, the second virial coefficient is $B_2^{hs} = 4V_I$ (calculated from eqn (3.2) and (3.4)), where $V_I = \frac{\pi}{6}\sigma^3$ is an effective interaction volume.

In general, the total interaction potential $U(r)$ has other terms in addition to the hard sphere contribution. The osmotic second virial coefficient B_2 may be calculated by the following equation:

$$B_2 = 4V_I + 2\pi \int_\sigma^\infty (1 - e^{-\beta[U(r) - U_{hs}(r)]}) r^2 \, dr \qquad (3.5)$$

which is derived from eqn (3.2). Also, the hydrodynamic coefficient may be calculated by the following expression, which is derived by assuming an additive hydrodynamic coupling:[52]

$$h_2 = \alpha_h V_I + 2\pi \int_\sigma^\infty (1 - e^{-\beta[U(r) - U_{hs}(r)]}) F\left(\frac{r}{\sigma}\right) r^2 \, dr \qquad (3.6)$$

where $F(x) = x^{-1} + O(x^{-4})$ is a function with the leading term of order x^{-1} and the other terms of order x^{-4} or higher. The coefficient α_h and the function $F(x)$ have been worked out by different treatments.[46,52] The most satisfactory values for α_h are 6.55 and 6.44 derived, respectively by Batchelor[57] and Felderhof.[58]

The interaction volume V_I and the equivalent hard-sphere diameter σ cannot be simply derived from experimental quantities such as the protein radius of gyration R_g or the protein specific volume v. As a first approximation, they may be assumed to depend upon the protein shape and solvation:[59,60]

$$V_I = f_s^3(v_0 + \delta v_w) M_0 N_A^{-1} \qquad (3.7)$$

where v_0 is the dry protein specific volume, v_w is the solvent specific volume, δ is the weight of the hydration solvent per weight of protein,[59] and f_s is a shape correction factor included to take into account a non spherical shape.[60]

The coefficient f_s has been derived in the case of oblate or prolate ellipsoid.[61] For instance, the BSA molecule has long been modelled as a prolate ellipsoid[62] with an axial ratio of 3.5.[60] In such case one obtains $f_s = 1.142$. However, such a model seems poor if compared with the known structure of the

analogous human serum albumin.[63] More recent SAXS data suggested the shape of an oblate ellipsoid with semiaxes of 1.7 and 4.2 nm.[64] In this second case, one obtains $f_s = 1.074$.

At 0% TFE, we measured a second virial coefficient of BSA $B_2^{0\%} = 1000 \pm 300$ nm^3. With the support of the literature data we may estimate the BSA interaction volume. If one takes $v_0 = 0.733$ cm^3 g^{-1},[62] $\delta = 0.34$,[65] $f_s = 1.141$, (prolate ellipsoid)[60] $M_0 = 66430$ g mol^{-1},[48] one obtains $V_I^{BSA} = 175$ nm^3. On the other hand, if one assumes the shape of an oblate ellipsoid ($f_s = 1.074$),[64] one obtains $V_I^{BSA} = 145$ nm^3. In any case, the correct value for the interaction volume is clearly affected by a correct estimate of the actual solvation, which is expressed by the parameter δ in expression (3.7). Since the value of $B_2^{0\%}$ is close to that of $4V_I^{BSA}$ (within the experimental error), one learns that steric repulsion plays a central role in the stabilization of the BSA solution, which is however endorsed by other interactions: $B_2^{0\%} > 4V_I^{BSA}$. Indeed, an electrostatic contribution was expected, since at the present pH the protein is electrically charged.[66]

The hydrodynamic coefficient accounts for the hydrodynamic effects, that is for the propagation on the motion of a particle of the disturbances due to the motion of the other particles.[46] It may be regarded as the coefficient of a concentration linear term in a collective friction coefficient. At 0% TFE, the hydrodynamic coefficient of BSA is $h_2^{0\%} = 2000 \pm 600$ nm^3. In the case of an ideal system with a repulsive hard sphere potential the hydrodynamic coefficient, calculated from expression (3.6) is $h_2^{HS} = \alpha_h V_I$.[46] Considerably higher values are typically and reasonably ascribed to electrostatic repulsion.[46,66] As a matter of fact, in the present case the value of $h_2^{0\%}$ is higher than that of a hard sphere system due to electrostatic interaction, as discussed for the second virial coefficient. Electrostatic repulsion becomes more important at moderate TFE concentration, likely due to a reduction of the dielectric constant.[67]

F Small angle X-ray scattering experiments

Small angle X-ray scattering (SAXS) experiments were performed on solutions of BSA concentration 1 mg ml^{-1} and 47 mg ml^{-1}, and at three TFE concentration: 0%, 10%, and 20% v/v.

The dependence of the scattered intensity upon the scattering vector q for a monodisperse system of non-spherical particles can be described, in the decoupling approximation, by the following expression:[68]

$$I(q) = \langle |F(q)|^2 \rangle \left(1 + \frac{|\langle F(q) \rangle|^2}{\langle |F(q)|^2 \rangle} [S(q) - 1] \right) \qquad (3.8)$$

where $F(q)$ is the scattering form factor, which is given by the spatial Fourier transform of the difference between the electron density of the particles and the solvent, and $S(q)$ is the interparticle structure factor, which depends upon the particle number concentration ρ, and the particle radial distribution function $g(r)$:

$$S(q) = 1 + 4\pi\rho \int_0^\infty [g(r) - 1] \frac{\sin(qr)}{qr} r^2 \, dr \qquad (3.9)$$

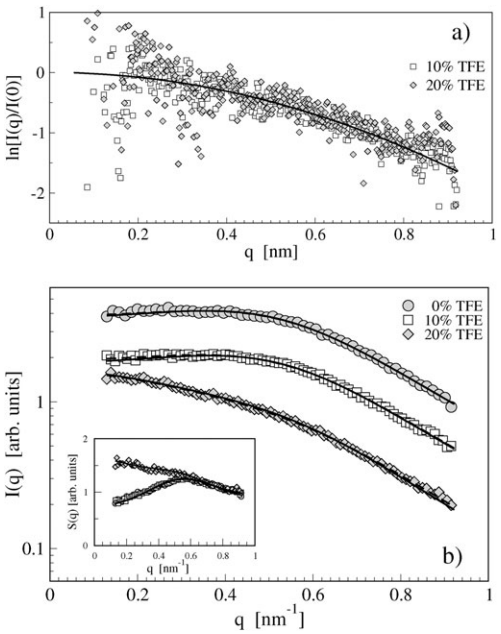

Fig. 2 Small angle X-ray scattering experiments at different TFE concentrations: 0% (circles), 10% (squares), 20% (diamonds). (a) Guinier plot of 1 mg ml^{-1} BSA in TFE–buffer solutions. (b) Structure functions of 47.5 mg ml^{-1} BSA in TFE–buffer solutions. Solid lines are the fitting curves. The curves are arbitrarily shifted to easily visualize the data. Inset: The structure factors of the main picture divided by the form factor $P(q)$.

The "intraparticle" form factor $P(q) = \langle |F(q)|^2 \rangle$ takes into account the shape of the particles. When the scattering vector q is low with respect to the reciprocal of the size of the molecule, one may use the typical Guinier expression and only one size parameter, the radius of gyration R_g:[68]

$$P(q) = \langle |F(q)|^2 \rangle = \exp\left\{ -\frac{1}{3} R_g^2 q^2 \right\} \qquad (3.10)$$

In such a case, the expression (3.8) can be simplified as:

$$I(q) = P(q)S(q) \qquad (3.11)$$

In order to measure the intraparticle form factor $P(q)$, we performed SAXS measurements at the dilute protein concentration of 1 mg ml^{-1} where protein interactions are negligible ($S(q) = 1$). The Guinier plot is shown in Fig. 2a for 10% and 20% TFE. In both cases, one obtains the same radius of gyration: $R_g = 2.4$ nm. This value is consistent with the oblate ellipsoidal shape of BSA, so that by assuming an axial ratio of 0.4[63,64] one obtains exactly the dry specific volume of BSA $v_0 = 0.733$ cm^3 g^{-1}.[62] Although our experiments probe low values of the scattering vector ($q < 1$ nm^{-1}), the Guinier approximation strictly holds for $q < 0.65$ nm^{-1}, that is $qR_g < 1.5$. However, no significant improvement is achieved in the interpolation of the experimental data if one uses the expression of a hard sphere, or an ellipsoid, or the Guinier expression, as appears clearly from the noise level of the data in Fig. 2a. Therefore, notwithstanding the actual shape of BSA, we may use expressions (3.10) and (3.11).

A second set of experiments was performed at the higher concentration of 47 mg ml^{-1} (Fig. 2b), in order to address the interparticle structure factor $S(q)$, and consequently the interaction potential.

The SAXS spectra of Fig. 2b at 0% and 10% TFE concentration were fit by using expressions (3.10) and (3.11) for the form factor, with the same radius of gyration R_g = 2.4 nm, and an appropriate choice of the interaction potential, which will be discussed below.

In Fig. 2b, the scattering curves at 0% and 10% TFE concentration have an identical shape, while the curve at 20% has a further increase at low scattering vectors. Although the radii of gyration measured on sample of 1 mg ml^{-1} protein concentration and 10% and 20% TFE concentration were identical, it is conceivable that at the higher concentration of 47 mg ml^{-1} the shape of the scattering curve may be due not only to a change in the protein interaction, but to a change in the protein shape and dimension, namely to a protein oligomerization.

G Light scattering at high BSA concentration

In order to solve this dilemma, we performed static and dynamic light scattering experiment at the same BSA and TFE concentrations of the X-ray scattering experiments. The intensity autocorrelation functions, displayed in Fig. 3, exhibit a single exponential decay with a correlation time τ that is directly proportional to the Rayleigh ratio R (inset of Fig. 3). The correlation time τ is proportional to the hydrodynamic radius R_h times the structure function $S(0)$, and the Rayleigh ratio R is proportional to the weight averaged molecular mass M_w times the structure function $S(0)$. An increase in the mass of a factor f (due *e.g.* to oligomerization) would yield an increase of the hydrodynamic radius of a factor much lower than f (depending upon the shape and the packing of the oligomers). We may ascribe a proportional increase of both correlation time τ and Rayleigh ratio R to the increase of the structure function $S(0)$, that is to the increase of the isothermal compressibility.[46] Therefore, the solution contains one single protein species with a comparable size and mass at each TFE concentration, and we may exclude further oligomerization.

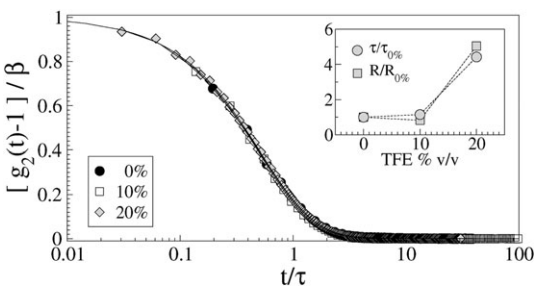

Fig. 3 Intensity autocorrelation functions of 47.5 mg ml^{-1} BSA in TFE–buffer solutions at different TFE concentrations: 0% (circles), 10% (squares), 20% (diamonds). Inset: normalized Rayleigh ratio R (squares) and correlation times τ (circles) *versus* TFE concentration.

H Suitable models for the interaction potential and the structure factor

In dilute aqueous electrolyte solutions, the protein interaction has been described in the framework of the Derjaguin–Landau–Verwey–Overbeek (DLVO) theory.[69] In this context, the protein molecules are modelled as charged, polarizable, hard spheres. The interaction consists of a hard sphere potential U_{hs} (as in expression (3.4)), a repulsive screened Coulomb electric potential U_{el}, and an attractive Hamaker dispersion potential U_{at}.

Screened Coulomb potential. The screened Coulomb potential is due to an ionic double-layer and can be expressed by the classic Yukawa potential:

$$\beta U_{el}(r) = Z^2 \frac{L_B}{r\left[1+\frac{\sigma}{2\lambda_D}\right]^2} \exp\left\{-\frac{(r-\sigma)}{\lambda_D}\right\} \qquad (3.12)$$

The above expression depends upon the hard-sphere diameter σ, and upon the Debye screening length $\lambda_D = (8\pi L_B N_A I)^{-0.5}$, where $L_B = e^2(4\pi\varepsilon k_B T)^{-1}$ is the Bijerrum length, N_A is the Avogadro number, e is the electron charge, Z is the number of electronic charges on the protein, k_B is the Boltzmann constant, T is the temperature, ε is the dielectric constant, and I is the ionic strength of the solution, which in the present experiments is 66 mM. At 0, 10 and 20%v/v, the Debye lengths are 1.365, 1.320 and 1.272 nm, respectively, and the Bijerrum lengths 0.715, 0.765 and 0.822 nm, respectively, by assuming a linear dependence of the dielectric constant upon the TFE concentration. At the present pH the protein is charged with slightly more than 10 electronic charges.[70,71]

Attractive potential. The attractive part of the potential U_{at} has an algebraic expression. However, in order to simplify the calculations it is often approximated with a negative Yukawa potential as in expression (3.12):

$$\beta U_{el}(r) = -J_{at}\frac{\sigma}{r}\exp\left\{-\frac{(r-\sigma)}{\lambda_{at}}\right\} \qquad (3.13)$$

For protein solution a suitable approximation would be a coefficient J_{at} of a few units and a characteristic length λ_{at} of about $\frac{1}{5}$ of the hard-sphere diameter σ, as found in experiments with lysozyme solutions.[72,73]

The DLVO potential contains a few essential ingredients of colloidal and protein interaction, however more refined treatments go beyond DLVO theory, by assuming other type of interactions, such as *e.g.* a contribution due to the solvent-accessible surface in the contact between two proteins.[56] On the other hand, the use of hard-sphere and one or more Yukawa potentials is a reasonable and convenient approach to the analysis of structure functions.[74]

Random phase approximation. Indeed, the structure factor $S(q)$ of a hard sphere system with a sum of Yukawa-type potentials $w(r)$ may be given an analytical solution in random phase approximation (RPA).[49] In the RPA, the pairwise potential $U(r)$ is divided into a short-range reference potential, which is usually the hard-sphere potential $U_{hs}(r)$, and a long-range perturbative potential $w(r)$. The structure factor $S(q)$ depends upon the structure factor of the reference

potential $S_0(q)$ and the Fourier transform of the perturbative potential $\hat{w}(q)$:

$$S(q)^{-1} = S_0(q)^{-1} + \rho\beta\hat{w}(q) \qquad (3.14)$$

Hard-sphere potential and structure factor. The hard-sphere structure factor $S_{hs}(q)$ is given in the Ornstein-Zernike approximation and with the Percus–Yevick closure relation by a well known expression, which depends only upon the protein concentration ρ and the hard-sphere diameter σ.[49]

Square-well potential and structure factor. In the context of protein solutions, the attraction due to a short range potential has been also modelled by the square well potential U_{sw}:

$$\beta U_{sw}(r) = \begin{cases} \infty, & r < \sigma \\ -u, & \sigma < r < \lambda\sigma \\ 0, & \lambda\sigma < r \end{cases} \qquad (3.15)$$

The Ornstein–Zernike equation in the Perkus–Yevick approximation can be solved for the square well potential to the first order in $(1 - \lambda^{-1})$,[75] to give an analytical expression for the structure factor $S_{sw}(q)$.[76]

I The nature of repulsive/attractive interactions

The SAXS spectra of Fig. 2b at 0% and 10% TFE concentration were fit by using expressions (3.10) and (3.11), with the same radius of gyration $R_g = 2.4$ nm. For the "interparticle" structure factor $S(q)$, we used expression (3.14) with different choices of the potential $w(r)$.

As a first attempt, we tried to fit the data by using the hard-sphere structure factor as reference ($S_0(q) = S_{hs}(q)$) and by taking into account the repulsive screened Coulomb potential of expression (3.12): $w(r) = U_{el}(r)$. This contribution is largely expected at the present low ionic strength.[60,64,65] However, it came out clearly that an attractive part should be added to the potential. Also, the addition of an attractive Yukawa potential in the reference part ($w(r) = U_{el}(r) + U_{at}(r)$) was not able to fit the shape of the data. Thus, we have used as reference the structure factor obtained from the square well potential: $S_0(q) = S_{sw}(q)$. The data at 0 and 10% TFE concentration were fit by the square-well structure factor $S_{sw}(q)$ with a hard-sphere diameter $\sigma = 7.6$ nm, a well depth $u = 11$ and a well width $\lambda = 1.00001$. A value of σ higher than the one calculated from the dry specific volume is sometimes attributed to sample polydispersity,[77] or also to an effective interaction volume V_I, which is affected by the non-spherical protein shape and by the solvation.[60] Note that the shape of the structure functions and the fitting parameters are alike for the samples in the thermodynamically stable phase, at 0% and 10% TFE concentration. At 20% TFE, the strength and the length of the attraction potential increases, and the bare square-well potential is not sufficient to fit the data. In such a case, we fit by using the RPA (eqn (3.14)) with the square-well potential as reference ($S_0(q) = S_{sw}(q)$) and the attractive Yukawa potential of the expression (3.13): $w(r) = U_{at}(r)$ (Fig. 2b). The fitting parameters are reported in Table 1. An analogous increase in attractive interaction by addition of TFE has been recently observed in lysozyme solutions, and explained as due to a perturbation of the proteins hydration shell and to the increasing of hydrophobic interactions.[14]

Table 1 Parameters from X-ray analysis (see expressions (3.12), (3.13), and (3.15))

c_{TFE} (%, v/v)	0	10	20
$U = U_{sw} + U_{at}$			
σ/nm	7.6	7.6	7.6
λ	1.00001	1.00001	1.00001
u	11.0	11.0	12.3
λ_{at}/nm	—	—	0.850
J_{at}	—	—	0.716
$U = U_{sw} + U_{at} + U_{el}$			
σ/nm	7.6	7.6	7.6
λ	1.00001	1.00001	1.00001
u	11.0	11.0	12.3
λ_{at}/nm	1.25	1.18	0.98
J_{at}	0.76	0.85	2.35
λ_D/nm	1.365	1.320	1.273
L_B/nm	0.715	0.765	0.822
Z	10	10	10

Although this result is qualitatively in agreement with the observation of the phase transition in BSA–TFE solutions, it is not able to explain quantitatively the experimental data of the second virial coefficient B_2. In particular the negative contribution to B_2 given by the square well potential (calculated by eqn (3.5)) overwhelms the positive contribution given by the bare steric repulsion.

Therefore, notwithstanding the quality of the fit with such a few parameters, we extended the analysis of the X-ray data by including in the perturbative part of RPA two Yukawa potentials: one is the electrostatic contribution of expression (3.12), and another is the attractive potential of expression (3.13): $w(r) = U_{el}(r) + U_{at}(r)$ (Fig. 2b). The same square-well structure factor $S_{sw}(q)$ was used as reference. In this analysis the parameters related to the electrostatic potential, namely the Debye length λ_D, the Bjerrum length L_B and the electric charge Z were fixed to the calculated values, as reported in Table 1. The fitting curves are displayed in Fig. 2b, and superimpose perfectly to those of the previous fit. As expected the addition of a repulsive term leads to an increase in the strength of the attraction term. However, also this analysis yields values of the virial coefficient that are well below the experimental findings.

The actual contribution of the potential $w(r)$ to the virial coefficient is marginal with respect to that of the hard-sphere potential $U_{hs}(r)$. The same effect applies *a fortiori* to the hydrodynamic coefficient h_2. Indeed, the integral of eqn (3.6), used to calculate h_2, contains the function $F(x)$, which is not included in the calculation of B_2 (eqn (3.5))). Therefore, if the contribution of $w(r)$ to B_2 is low the contribution to h_2 will be lower.

The values of the hard sphere diameter σ obtained by the analysis of X-ray data are higher than those obtained from the dry volume of BSA ($\sigma = 5.36$ nm).[71] Interestingly, the second virial coefficients related to the hard-sphere repulsion ($B_2^{hs} = 920$ nm^3) have values much closer to the experimental ones. Also, it is worth noting that the values of the hard sphere radii match the value of the hydrodynamic radius obtained at

0% TFE concentration (R_h = 3.8 nm). In an oblate or prolate ellipsoid the ratio between the hydrodynamic radius R_h and the radius of gyration is equivalent to the ratio between the hard-sphere equivalent radius $\sigma/2$ (used to calculate the interaction volume V_I) and the radius of gyration.[59,61] For ellipsoid with an axial ratio between 0.25 and 4, the difference between R_h and $\sigma/2$ is less than 1%. In addition, the hydrodynamic radius is affected by the solvation of the molecules analogously to the quantity $\sigma/2$ (see expression (3.7)). Therefore, it seems reasonable to use the hydrodynamic radius at infinite dilution R_h to estimate the interaction volumes V_I, and the corresponding contribution to the second virial coefficient ($4V_I$). In this pespective, we may calculate the quantity $V_I^{(h)} = \frac{4}{3}\pi R_h^3$ from the measured hydrodynamic coefficient, and compare it with the measured virial coefficient. At the TFE concentrations of 0%, 4.3% and 13.3%, we measured $4V_I^{(h)}$ = 920, 1200 and 1600, respectively, and B_2 = 1000, 1400 and 1800, respectively. If one considers that the experimental uncertanty in these values is higher than 10%, they can be taken as equivalent, thus strengthening the evidence that steric repulsion and solvation are determinant for the thermodynamic stabilty of these solutions.

In summary, from the X-ray data analysis and from the careful inspection of light scattering data we derive the following robust results: (i) the steric repulsion plays a main role in the stabilization of protein solutions, and the addition of TFE at low concentration increases the solution stability with a correlated increase in the protein solvation; (ii) the onset of instability is due to the prevalence of an attractive contribution to the overall potential, which cannot be explained in the context of DLVO interaction. This overwhelming attraction is likely long-range, since the X-ray structure function in the range above 0.1 nm^{-1} is not able to identify it.[78]

J Far-UV circular dichroism experiments

The far-UV circular dichroism spectra were measured at different TFE concentrations (0–20% v/v) to study conformational effects on the protein secondary structure. In the shape of the far-UV spectra tiny differences could be noticed by varying TFE concentrations (Fig. 4a). BSA secondary structure remains mostly unchanged upon addition of TFE, as evidenced by the spectra, which are typical of a protein with a predominant α-helix structure.[79–81] Differences among spectra are more evident close to the minima. Thus, the ratio between the minimum at 209 nm and the minimum at 222 nm is displayed in the inset of Fig. 4a to mark the effect of TFE on the shape of the far-UV spectra. We observe only moderate changes of this ratio.

K Near-UV circular dichroism experiments

The changes in the protein tertiary structure due to the presence of TFE were studied by measuring near-UV circular dichroism spectra (Fig. 4b). Tryptophans, as well as tyrosines, phenylalanines and disulfide bridges, appear to be involved in these conformational changes. Indeed, the main contribution to CD signal close to 300 nm arises from tryptophans, while the lower part of the spectrum is more predominantly due to

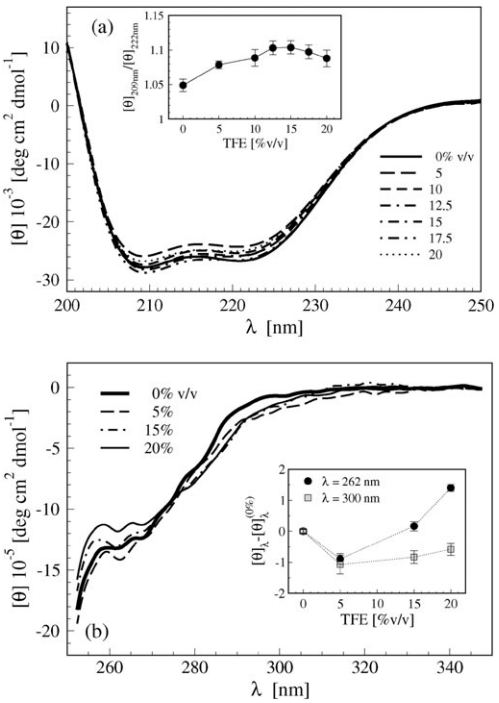

Fig. 4 (a) Far-UV CD spectra of 2.8 μM BSA in TFE–buffer solutions at different TFE concentrations. Inset: Ratio between the CD values at 209 and 222 nm. (b) Near-UV CD spectra of 11.3 μM BSA in TFE–buffer solutions at different TFE concentrations: 0% (bold solid line), 5% (dashed line), 15% (dashed and dotted line), 20% (solid line). Inset: CD values at 262 nm (circles) and 300 nm (squares).

tyrosines, around 280 nm, and phenylalanines, and disulfide bridges, around 262 nm.[79] The results show that the addition of TFE, even at low concentration (5% v/v), causes moderate conformational changes (inset of Fig. 4b). At higher TFE concentrations, the signal at 262 nm (related to phenylalanines) still changes, while the 300 nm signal (related to the environment of tryptophans) exhibits a much lower variation. However, such variations are limited within a few percent, and they should not be related to a significant loss of native conformation, as in the case of BSA unfolding.[82]

L Intrinsic fluorescence experiments

Intrinsic fluorescence emission spectra from tryptophan residues were measured at different TFE concentrations (0–30% v/v) to study local conformational effects on the protein structure (Fig. 5a). Intrinsic fluorescence comes from the residue Trp134, located in proximity of the protein surface (domain IB), and the residue Trp212, located in an internal part of the protein (domain IIA).[83] The quantum yield of tryptophans decreases as TFE is increased from 0 to 10% v/v (Fig. 5). Saturation is reached at higher concentrations where further changes are not appreciated any more. The maximum of the emission band blue-shifts from 340 nm to 332 nm going from 0 to 10% v/v TFE, and keeps unchanged for higher TFE concentrations, in tune with the quantum yield (Fig. 5b). In the case of BSA-unfolding, the tryptophan environment would become more polar, causing a red-shift in the fluorescence emission.[84] The emission maxima obtained from tryptophan solutions at different TFE concentrations are also reported as

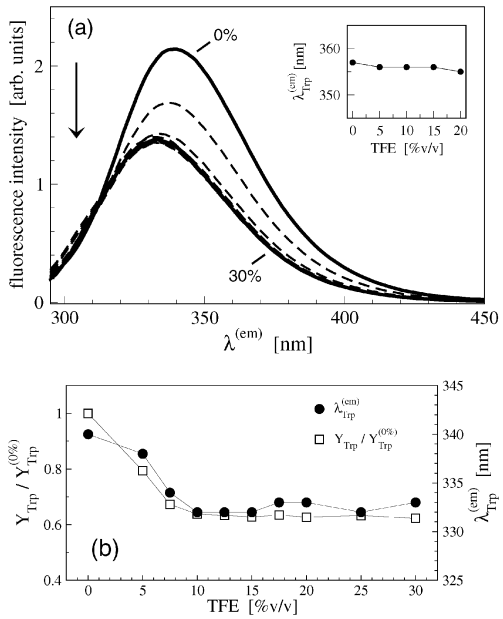

Fig. 5 (a) Intrinsic fluorescence emission spectra of 2 μM BSA in TFE–buffer solutions at increasing TFE concentrations, as indicated by the arrow: 0% (solid line); 5%, 7.5%, 10%, 12.5%, 15%, 17.5%, 20%, 25% (dashed lines); 30% (solid line). Inset: Maximum emission wavelength of free tryptophan in TFE–buffer solutions. (b) Maximum emission wavelength (circles) and quantum yield (squares) obtained from intrinsic fluorescence experiments.

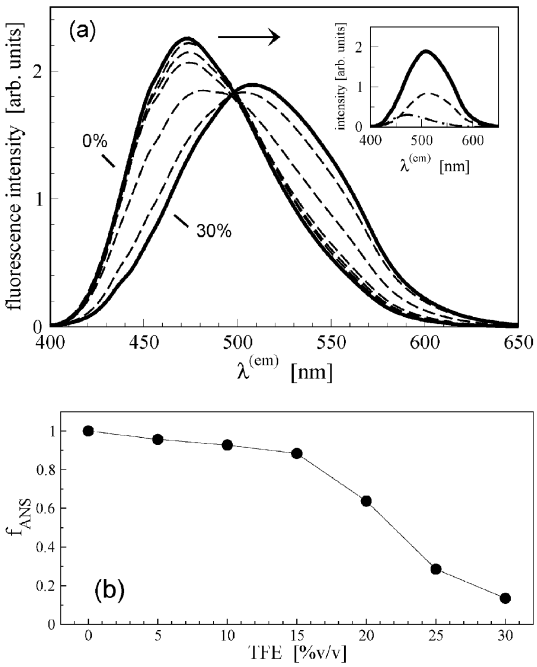

Fig. 6 (a) ANS fluorescence emission spectra of 2 μM BSA in TFE–buffer solutions at increasing TFE concentrations as indicated by the arrow: 0% (solid line); 5%, 10%, 15%, 20%, 25% (dashed lines); 30% (solid line). Inset: example of spectrum deconvolution; ANS emission spectrum at 30% TFE with 2 μM BSA (solid line), ANS emission spectrum at 0% TFE with 2 μM BSA (dashed line), ANS emission spectrum at 30% TFE without BSA (dotted line). (b) Fraction of solvent excluded ANS from ANS fluorescence experiments.

an indication of the behaviour of the fluorophore when fully exposed to the solvent (inset of Fig. 5a). In the present experiments, the tryptophan environment becomes more hydrophobic upon TFE addition.[85] We may ascribe such an effect to a structural reorganization in a less solvent-exposed conformation. Remarkably, the BSA unfolding is ruled out, thus confirming and strengthening CD data.

M ANS fluorescence experiments

The fluorescence emission spectra arising from molecules of an external probe, the fluorophore ANS, were measured at different TFE concentrations (0–30% v/v) to study global conformational changes. The source of ANS interaction with BSA, which is still unclear, may be due to both electrostatic and hydrophobic interactions.[86] Although ANS may bind to different sites in the BSA molecules,[86] ANS exhibits an appreciable fluorescence when bound to about 5 sites,[87] likely located within the hydrophobic cleft of BSA. Indeed, ANS fluorescence has been used for denaturation studies, since fluorescence is quenched in aqueous solution or other polar environment.[86,87] Fig. 6a shows the emission spectra of ANS in the presence of BSA at different TFE concentrations. ANS interacting with BSA shows an emission maximum around 470 nm (solid line in Fig. 6a). Free ANS fluorescence emission in phosphate buffer–TFE solutions is characterized by an emission maximum around 520 nm at each TFE concentration (data not shown). The presence in the ANS–BSA spectra of an isoemissive point at 500 nm (Fig. 6a) suggests that the emission comes from two different populations of ANS molecules, one bound to the protein in the hydrophobic sites, and another dissolved in the solvent or simply exposed to the solvent. Therefore, according to this model, the data at different TFE concentrations were analyzed by data fitting with a linear combination of two components: (1) the ANS emission spectrum at 0% TFE concentration and in the presence of BSA, taken as a reference for the ANS–BSA complex; and (2) the ANS emission spectrum at each given TFE concentration without BSA, representing the free/solvent-exposed ANS molecules. An example of this deconvolution is displayed in the inset of Fig. 6a for 30% v/v TFE concentration. The weight of the former component, f_{ANS}, gives a measure of the fraction of ANS molecules interacting with BSA or bound to the hydrophobic sites. It is worth noting that the present experiments are performed with an excess of ANS, in order to overcome any influence of TFE on the affinity of ANS for BSA, as observed in other alcohol–water solutions.[88] Therefore, the decrease of the quantity f_{ANS} signs a molecular conformational change, likely related to the loosening of the BSA hydrophobic cleft (Fig. 6b). Interestingly, such a change in the molecular conformation is well correlated with the emergence of attractive interactions, as revealed by light scattering data.

N Conformational re-arrangement in the stable phase

At low TFE concentrations, BSA molecules exhibit soft structural re-arrangements. The more significant change is observed in the environment of tryptophan residues, and most

likely of the more external residue Trp134.[81,83] This is clearly shown by the measurements of the near-UV CD spectra (Fig. 4b) as well as the intrinsic fluorescence spectra (Fig. 5). In particular, the blue-shift of the fluorescence emission maximum marks the occurrence of a less polar environment.[83] Therefore, one may argue that the presence of TFE leads to a more compact tertiary structure, or that TFE molecules preferentially solvate the tryptophan environment.[39] The latter occurrence is particularly sound, for the following reasons: (i) the changes in tryptophan fluorescence are correlated with the apparent swelling of the hydrodynamic radius shown in the inset of Fig. 1b; (ii) while the main conformational changes related to the tryptophan environment occur below 10%, no changes are observed at higher TFE concentration, when a loosening of native conformation occurs, as marked by ANS fluorescence (Fig. 6); (iii) the apparent weight averaged molecular mass M_w of BSA exhibits a slight increase in the stable phase (inset of Fig. 1a). Indeed, the ratio between the apparent and the actual molecular mass is related to the preferential hydration of the protein by a co-solute in a mixed solvent.[89] Although the present results are blurred by the considerable experimental uncertainty (Fig. 1a), they are reminiscent of the classic results of Inoue and Timascheff on the preferential hydration of β-lactoglobulin by 2-chloroethanol.[89]

The far-UV CD spectra reveals very tiny changes related to the secondary structure (Fig. 2). The spectra have two minima, as typically observed in BSA, and more in generally in proteins with a high amount of α-helical secondary structure.[80] The increase in the ratio between the two minima (Fig. 4a) may be due to a strengthening of the α-helical secondary structure, which is a known effect of TFE on proteins and peptides.[20,22–24] However, we stress that these changes in the shape of CD spectra are within a few percent, and we are observing marginal effects.

O Conformational changes across the threshold

The mentioned changes of protein conformation occur essentially in the low range of TFE concentrations. In other words, the bare addition of small amount of TFE causes moderate conformational changes, likely to be related to the preferential hydration of protein molecules by TFE, and, most remarkably, along with these changes, the thermodynamic stability is enhanced by strengthening repulsive interaction. At higher TFE concentration, the onset of thermodynamic instability is not correlated with dramatic changes in the secondary structures or in the tryptophan environment. Indeed, the changes in the tryptophan signals displayed in Fig. 4b and 5b occurs within a TFE concentration of about 10%, while the changes in the signals displayed in Fig. 1c and 6b exhibit a more sigmoidal shape. The crossover from repulsive to attractive interaction (Fig. 1c) is, however, accompanied by the variation in the signal of ANS fluorescence (Fig. 6b), which is related to a more-conspicuous exposure of the hydrophobic cleft to the solvent. Coherent with such a variation, a change in near-UV CD signal is also evident in the region of the spectrum arising from phenylalanine residues and disulfide bridges (inset of Fig. 4b), suggesting a slight loosening of the tertiary structure. Indeed, while the tryptophan signal is quite specific, phenylalanines are jumbled in the whole sequence, and thus they can probe less-selectively any conformational change.

IV. Conclusions

A TFE operates as a conformational effector

The present paper reports a comprehensive experimental work on the effect of TFE on the thermodynamic and conformational stability of BSA. Recently it has been reported that for lysozyme at relatively low TFE concentrations (less than 10% v/v) TFE stabilizes tertiary structure, while for higher concentrations (up to 50% v/v) denaturation and loss of structural organization occur.[30] Also, the calorimetric profiles of BSA thermal unfolding at different TFE concentrations show that the BSA conformation is slightly stabilized at low TFE concentrations, and moderately destabilized above 10% TFE, consistent with our results.[81] The present results show that TFE affects BSA conformations, at low and moderate concentrations, through the preferential hydration of protein surface. This local, molecular interaction between TFE and the protein alters the activity of the protein in solution.[90] Hence, TFE acts as a conformational effector, since it affects the solvent-mediated interactions between proteins through a direct mechanism. The transition from a stable to a metastable phase seems due not to a change in the TFE action on the protein, but to a balance of the interactions involved.

Consistently, from the analysis of scattering data, we found that both steric repulsion and solvation are pivotal in determining the interparticle interaction and the thermodynamic properties. The onset of instability and the prevalence of attractive interactions upon addition of TFE cannot be explained in the frame of classic DLVO theory.

As a concluding remark, we argue that the stabilization of the protein structure, *via* selective hydration, suggests a strengthening of the hydrophobic interaction.[90] The latter covers many length scales and affects intra- as well as intermolecular forces, since the solvent plays a role in both of them.[4,90] At the same time, the addition of TFE implies a reduction of the dielectric constant and an enhancement of electrostatic repulsion. The onset of instability is due to a prevalence of the hydrophobic attraction over repulsion, upon slight, yet basic, molecular changes towards a more solvent-exposed conformation.[91,92]

This work represents an effort to study the protein–protein interaction and the molecular conformational details as a whole. It aims to show that the thermodynamic properties are strictly connected to the conformational space visited by a protein. Even tiny differences in the structural details can lead to a change in the interaction potential and as a consequence in the thermodynamic observables. Therefore, the results of the present work are two-fold. On one hand, we obtained a deeper comprehension of the mechanism through which TFE operates in protein solutions. On the other hand, we explained, in the case of a model protein and an interesting co-solute, how small changes in the conformational properties can trigger the prevalence of attractive intermolecular interactions.

Such a correlation between conformational and thermodynamic stability emphasizes the existing link between protein structural details and protein interactions in protein solutions.

Acknowledgements

We thank D. Bulone, F. Cavalieri, L. Cordone, D. Giacomazza, R. Noto, G. Paradossi and S. Raccosta for relevant discussions and collaborations. This work was partially supported by the Italian National Research Council through the project *Intermolecular interaction in protein metastable solution*.

References

1 J. M. Prausnitz, *Pure Appl. Chem.*, 2003, **75**, 859–873.
2 S. Frokjaer and D. E. Otzen, *Nat. Rev. Drug Discovery*, 2005, **4**, 298–306.
3 D. W. Urry, *What Sustains Life? Consilient Mechanisms for Protein-Based Machines and Materials*, Springer—Science & Business Media, LLC, New York, 2006.
4 M. Manno, A. Emanuele, V. Martorana, P. L. San Biagio, D. Bulone, M. B. Palma-Vittorelli, D. T. McPherson, J. Xu, T. M. Parker and D. W. Urry, *Biopolymers*, 2001, **59**, 51–64.
5 C. M. Dobson, *Nature*, 2003, **426**, 884–890.
6 A. George and W. W. Wilson, *Acta Crystallogr.*, 1994, **50**, 361–365.
7 D. Rosenbaum, P. C. Zamora and C. F. Zukoski, *Phys. Rev. Lett.*, 1996, **76**(1), 150–153.
8 W. Liu, D. Bratko, J. M. Prausnitz and H. W. Blanch, *Biophys. Chem.*, 2004, **107**, 289–298.
9 S. Grudzielanek, R. Jansen and R. Winter, *J. Mol. Biol.*, 2005, **351**, 879–894.
10 M. Manno, E. F. Craparo, A. Podestà, D. Bulone, R. Carrotta, V. Martorana, G. Tiana and P. L. San Biagio, *J. Mol. Biol.*, 2007, **366**, 258–274.
11 R. Carrotta, M. Manno, D. Bulone, V. Martorana and P. L. San Biagio, *J. Biol. Chem.*, 2005, **280**, 30001–30008.
12 J. P. Schmittschmitt and J. M. Scholtz, *Protein Sci.*, 2003, **12**, 2374–2378.
13 N. Javid, K. Vogtt, C. Krywka, M. Tolan and R. Winter, *Phys. Rev. Lett.*, 2007, **99**, 028101-1–028101-4.
14 N. Javid, K. Vogtt, C. Krywka, M. Tolan and R. Winter, *ChemPhysChem*, 2007, **8**, 679–689.
15 A. Lomakin, N. Asherie and G. B. Benedek, *Proc. Natl. Acad. Sci. U. S. A.*, 1999, **96**, 9465–9468.
16 E. Y. Chi, S. Krishnan, B. S. Kendrik, B. S. Chang, J. F. Carpenter and T. W. Randolph, *Protein Sci.*, 2003, **12**, 903–913.
17 M. Manno, P. L. San Biagio and M. U. Palma, *Proteins: Struct., Funct., Bioinf.*, 2004, **55**, 169–176.
18 M. Calamai, F. Chiti and C. M. Dobson, *Biophys. J.*, 2005, **89**, 4201–4210.
19 J. J. Valente, K. S. Verma, M. C. Manning, W. W. Wilson and C. Henry, *Biophys. J.*, 2005, **89**, 4211–4218.
20 J. W. Nelson and N. R. Kallenbach, *Biochemistry*, 1989, **28**, 5256–5261.
21 A. Dong, J. Matsuura, M. C. Manning and J. F. Carpenter, *Arch. Biochem. Biophys.*, 1998, **335**, 275–281.
22 M. Buck, H. Schwalbe and C. M. Dobson, *Biochemistry*, 1995, **34**, 13219–13232.
23 K. Shiraki, K. Nishikawa and Y. Goto, *J. Mol. Biol.*, 1995, **245**, 180–194.
24 Y. Luo and R. L. Baldwin, *J. Mol. Biol.*, 1998, **279**, 49–57.
25 D. Hamada, F. Chiti, J. I. Guijarro, M. Kataoka, N. Taddei and C. M. Dobson, *Nat. Struct. Biol.*, 2000, **7**, 58–61.
26 H. Lu, M. Buck, S. E. Radford and C. M. Dobson, *J. Mol. Biol.*, 1997, **265**, 112–117.
27 F. Chiti, N. Taddei, P. Webster, D. Hamada, T. Fiaschi, G. Ramponi and C. M. Dobson, *Nat. Struct. Biol.*, 1999, **6**, 380–387.
28 A. Kundu and N. Kishore, *Biophys. Chem.*, 2004, **109**, 427–442.
29 P. Del Vecchio, G. Graziano, V. Granata, G. Barone, L. Mandrich, M. Rossi and G. Manco, *Biophys. Chem.*, 2003, **104**, 407–415.
30 J. Povey, C. M. Smales, S. J. Hassard and M. J. Howard, *J. Struct. Biol.*, 2007, **157**, 329–338.
31 V. E. Bychkova, A. E. Dujsekina, S. I. Klenin, E. I. Tiktopulo, V. N. Uversky and O. B. Ptitsyn, *Biochemistry*, 1996, **35**, 6058–6063.
32 G. Damaschun, H. Damaschun, K. Gast and D. Zirwer, *J. Mol. Biol.*, 1999, **291**, 715–725.
33 K. Gast, D. Zirwer, M. Mller-Frohne and G. Damaschun, *Protein Sci.*, 1999, **8**, 625–634.
34 M. Buck, S. E. Radford and C. M. Dobson, *Biochemistry*, 1993, **32**, 669–678.
35 M. Hoshino, Y. Hagihara, D. Hamada, M. Kataoka and Y. Goto, *FEBS Lett.*, 1997, **416**, 72–76.
36 D. Roccatano, G. Colombo, M. Fioroni and A. E. Mark, *Proc. Natl. Acad. Sci. U. S. A.*, 2002, **99**, 12179–12184.
37 S. Cinelli, G. Onori and A. Santucci, *J. Phys. Chem. B*, 1997, **101**, 8029–8034.
38 P. D. Thomas and K. A. Dill, *Protein Sci.*, 1993, **2**, 2050–2065.
39 R. Rajan and P. Balaram, *Int. J. Peptide Protein Res.*, 1996, **48**, 328–336.
40 R. Walgers, T. C. Lee and A. Cammers-Goodwin, *J. Am. Chem. Soc.*, 1998, **120**, 5073–5079.
41 S. Kuprin, A. Gräslund, A. Ehrenberg and M. H. J. Koch, *Biochem. Biophys. Res. Commun.*, 1995, **217**, 1151–1156.
42 T. Takamuku, T. Kumai, K. Yoshida, T. Otomo and T. Yamaguchi, *J. Phys. Chem. A*, 2005, **109**, 7667–7676.
43 K. R. Harris, P. J. Newitt and Z. J. Derlacki, *J. Chem. Soc., Faraday Trans.*, 1998, **94**, 1963–1970.
44 H. Reiersen and A. R. Rees, *Protein Eng.*, 2000, **13**, 739–743.
45 D.-P. Hong, M. Hoshino, R. Kuboi and Y. Goto, *J. Am. Chem. Soc.*, 1999, **121**, 8427–8433.
46 K. S. Schmitz, *An Introduction to Dynamic Light Scattering by Macromolecules*, Academic Press, Inc., San Diego, 1990.
47 M. B. Huglin, in *Light Scattering from Polymer Solutions*, ed. M. B. Huglin, Academic Press, New York and London, 1972.
48 K. Hirayama, S. Akashi, M. Furuya and K. Fukuhara, *Biochem. Biophys. Res. Commun.*, 1990, **173**, 639–646.
49 J. P. Hansen and I. R. McDonald, *Theory of Simple Liquids*, Academic Press, London, New York, San Diego, 1986.
50 M. Manno, C. Xiao, D. Bulone, V. Martorana and P. L. San Biagio, *Phys. Rev. E*, 2003, **68**, 011904-1–011904-11.
51 M. Manno, D. Bulone, V. Martorana and P. L. San Biagio, *J. Phys.: Condens. Matter*, 2004, **16**, S5023–S5033.
52 P. N. Pusey, in *Liquid Freezing and Glass Transition*, ed. J. P. Hansen, D. Levesque and J. Zinn-Justine, North Holland Elsevier Science Publishers B.V., Amsterdam, 1992.
53 G. Gente and C. L. Mesa, *J. Sol. Chem.*, 2000, **29**, 1159–1171.
54 Y. S. Oh and C. S. J. Johnson, *J. Chem. Phys.*, 1981, **74**, 2717–2720.
55 R. Itri, W. Caetano, L. R. S. Barbosa and M. S. Baptista, *Braz. J. Phys.*, 2004, **34**, 58–63.
56 R. A. Curtis, C. Steinbrecher, M. Heinemann, H. W. Blanch and J. M. Prausnitz, *Biophys. Chem.*, 2002, **98**, 249–265.
57 G. K. J. Batchelor, *J. Fluid. Mech.*, 1976, **74**, 1–29.
58 B. U. J. Felderhof, *J. Phys. A*, 1978, **11**, 929–937.
59 C. Tanford, *Physical Chemistry of Macromolecules*, Wiley, New York, 1961.
60 R. Nossal, C. J. Glinka and S.-H. Chen, *Biopolymers*, 1986, **25**, 1157–1175.
61 A. Isihara, *J. Chem. Phys.*, 1950, **18**, 1446–1449.
62 H. A. Sheraga and L. Mandelkern, *J. Am. Chem. Soc.*, 1953, **75**, 179–184.
63 M. L. Ferrer, R. Duchowicz, B. Carrasco, J. Garcia de la Torre and A. U. A. Na, *Biophys. J.*, 2001, **80**, 2422–2430.
64 F. Zhang, M. W. A. Skoda, R. M. J. Jacobs, R. A. Martin, C. M. Martin and F. Schreiber, *J. Phys. Chem. B*, 2007, **111**, 251–259.
65 D. Bendedouch and S.-H. Chen, *J. Phys. Chem.*, 1983, **87**, 1473–1477.
66 P. Doherty and G. B. Benedek, *J. Chem. Phys.*, 1974, **61**, 5426–5434.
67 D. G. Neal, D. Purich and D. S. Cannell, *J. Chem. Phys.*, 1984, **80**, 3469–3477.

68 L. A. Feigin and D. I. Svergun, *Structure Analysis by Small-Angle X-Ray and Neutron Scattering*, Plenum, New York, 1987.
69 E. J. W. Verwey and J. T. G. Overbeck, *Theory of the Stability of Lyophobic Colloids*, Elsevier, New York, 1948.
70 V. L. Vilker, C. K. Colton and K. A. Smith, *J. Colloid Interface Sci.*, 1981, **79**, 548–566.
71 A. Minton and H. Edelhoch, *Biopolymers*, 1982, **21**, 451–458.
72 M. Malfois, F. Bonnet, A. Tardieu and L. Belloni, *J. Chem. Phys.*, 1996, **105**, 3290–3300.
73 A. Tardieu, A. Le Verge, M. Malfois, F. Bonnet, S. Finet, M. Riès-Kautt and L. Belloni, *J. Cryst. Growth*, 1999, **196**, 193–203.
74 M. Broccio, D. Costa, Y. Liu and S.-H. Chen, *J. Chem. Phys.*, 2006, **124**, 084501-1–084501-9.
75 Y. C. Liu, S. H. Chen and J. S. Huang, *Phys. Rev. E*, 1996, **54**(2), 1698–1708.
76 W. R. Chen, S.-H. Chen and F. Mallamace, *Phys. Rev. E*, 2002, **66**, 021403-1–021403-12.
77 J. S. Pedersen, *Phys. Rev. B*, 1993, **47**, 657–665.
78 Y. Liu, E. Fratini, P. Baglioni, W. R. Chen and S.-H. Chen, *Phys. Rev. Lett.*, 2005, **95**, 118102-1–118102-4.
79 G. D. Fasman, *Circular Dichroism and the Conformational Analysis of Biomolecules*, Plenum Press, New York, 1996.
80 N. El Kadi, N. Taulier, J. Y. L. Huérou, M. Gindre, W. Urbach, I. Nwigwe, P. C. Kahn and M. Waks, *Biophys. J.*, 2006, **91**, 3397–3404.
81 T. Banerjee and N. Kishore, *Biopolymers*, 2005, **78**, 78–86.
82 C. Sun, J. Yang, X. Wu, X. Huang, F. Wang and S. Liu, *Biophys. J.*, 2005, **88**, 3518–3524.
83 Y. Moriyama, D. Ohta, K. Hachiya, Y. Mitsui and K. Takeda, *J. Protein Chem.*, 1996, **15**, 265–271.
84 P. M. Viallet, T. Vo-Dinh, A.-C. Ribou, J. Vigo and J.-M. Salmon, *J. Protein Chem.*, 2000, **19**, 431–439.
85 J. R. Lakowicz, *Principles of Fluorescence Spectroscopy*, Kluwer Academic/Plenum Publishers, New York, 1999.
86 D. Matulis, C. G. Baumann, V. A. Bloomfield and R. E. Lovrien, *Biopolymers*, 1999, **49**, 451–458.
87 E. Daniel and G. Weber, *Biochemistry*, 1966, **5**, 1893–1900.
88 N. A. Avdulov, S. V. Chochina, V. A. Daragan, F. Schroeder, K. H. Mayo and W. G. Wood, *Biochemistry*, 1996, **35**, 340–347.
89 I. I. S. N. Timasheff, *J. Am. Chem. Soc.*, 1968, **90**, 1890–1897.
90 S. N. Timasheff, *Proc. Natl. Acad. Sci. U. S. A.*, 2002, **99**, 9721–9726.
91 L. Cordone, A. Cupane and E. Vitrano, *J. Mol. Liq.*, 1989, **42**, 213–229.
92 R. Giordano, F. Wanderlingh, L. Cordone and A. Cupane, *Nuovo Cimento*, 1983, **2D**, 47–54.

